JOURNAL OF GUIDANCE, CONTROL, AND DYNAMICS
Vol. 25, No. 5, September–October 2002

Method for Calculating Collision Probability Between a Satellite and a Space Tether

Russell P. Patera*
The Aerospace Corporation, Los Angeles, California 90009-2957

A method for calculating the collision probability between an orbiting object and a space tether, given the respective state vectors and error covariance matrices, has been developed. The methodology employs an efficient computational scheme that was used successfully in predicting the collision hazard for asymmetrical satellites. The tether is modeled as a very long, slender body having a predefined serpentine shape with a circular cross section. The colliding space object is assumed to be spherical in shape. Analytical techniques are used to reduce the collision prediction problem to that of integrating a two-dimensional symmetric probability density over a region representing the collision cross section of the tether and space object. The symmetric form of the probability density enables the two-dimensional integral to be reduced to a one-dimensional path integral that permits easy numerical implementation. Test case results indicate collision probabilities significantly higher than satellite–satellite collision probabilities.

Nomenclature

a	=	auxiliary parameter
c	=	auxiliary parameter
d	=	auxiliary parameter
e	=	auxiliary parameter
f	=	auxiliary parameter
g	=	auxiliary parameter
h	=	two-dimensional probability density
I	=	value of integrand in Eq. (24)
J	=	subinterval number for contour integration
n	=	number of propagation steps
P	=	collision probability
q_i	=	points defining perimeter of hard-body area
q_{ir}	=	q_i after a rotation to diagonalize the probability density
q_{irs}	=	q_{ir} after a scale change to symmetrize the probability density
r	=	radial coordinate in symmetrized encounter plane
$s1, s2$	=	integration contours
T	=	rotation matrix used to diagonalize the two-dimensional probability density
U	=	transformation matrix from encounter to diagonal frame
$u(\boldsymbol{x})$	=	step function defining hard-body area
$\boldsymbol{X}_n$	=	vector defining integration subinterval
$\boldsymbol{x}_1, \boldsymbol{x}_2$	=	adjacent points on the hard-body perimeter
x, y, z	=	coordinates used in probability density function
α	=	coefficient defining probability density
β	=	coefficient defining probability density
θ	=	contour integration parameter
$\rho(\boldsymbol{x})$	=	three-dimensional probability density function
$\sigma_{x,y,z}$	=	probability density standard deviations for each axis
φ	=	rotation angle to eliminate the cross term in the two-dimensional probability density

Received 26 March 2001; revision received 28 March 2002; accepted for publication 29 April 2002.

*Senior Engineering Specialist, Center for Orbital and Reentry Debris Studies, P.O. Box 92957.

Introduction

SPACE tethers have been proposed as an inexpensive method for raising a satellite to its operational orbit. Tethers have also been proposed for lowering a satellite's orbit for disposal at the end of life. The long length (several kilometers) and vertical configuration of space tethers results in higher collision probabilities than experienced by typical satellites. The collision hazard posed by space tethers has been recognized, and special guidelines were added to the NASA Safety Standard 1740.14 (Ref. 1). These guidelines recommend analyzing the collision risk for tethers for both intact and severed conditions. The long-term debris impact rate for a particular space tether, given the density of debris objects in the tether's orbital altitude range, has been assessed.[2] However, a method to quantify the collision risk for individual encounters between space objects and tether systems is needed.

Significant progress has been made in space object collision probability calculation in recent years. Chan showed that the relative positional error covariance matrix could be obtained by simply adding the error covariance matrices of the respective colliding space objects.[3] The combined error covariance matrix has an associated three-dimensional probability density function that represents the uncertainty in relative position between the two objects. The collision problem permits integrating the dimension parallel to the relative velocity vector, thereby reducing the problem to two dimensions. The collision probability can, thus, be obtained by integrating the two-dimensional probability density over a hard-body region in a plane normal to the relative velocity vector referred to as the encounter frame. Because the attitude of each space object is not known, the hard-body region is circular with a diameter equal to the sum of the characteristic sizes of the space objects. This two-dimensional integral method of calculating the collision probability was found to be in agreement with Monte Carlo simulations for close encounter configurations.[4]

The two-dimensional integral can be reduced to a one-dimensional integral involving the error function.[3–6] However, the error function formulation is not very useful due to numerical accuracy and computational efficiency problems.[3,5] Nevertheless, when a coordinate rotation and scale change are used, the problem was reduced to a one-dimensional closed contour integral involving a simple exponential function.[7] This one-dimensional contour integral permits the treatment of asymmetric space objects in a simple fashion that is amenable to computer implementation.

The contour integral methodology was recently used to treat asymmetric satellites by using polygonal shapes to approximate satellite components.[7] Nevertheless, a more appropriate calculation method is needed for space tethers because of their arbitrary shape, long length, and narrow diameter. The objective of the current work

is to develop such a method. Specialized processing required for tether geometry is presented. The method was implemented in a computer simulation, and results from several numerical examples are presented.

Methodology

Tethers can be deployed from a parent satellite and may have a tip mass to enhance gravity gradient stabilization. Tethers may also be used to link several satellites. A significant amount of analysis has been reported on tether configuration, dynamics, and control.[8–11] Once the shape and orientation of the tether is determined, a method of calculating its collision probability with a space object can proceed.

The collision probability calculation for a parent satellite/tether system is separated into collision probability for the parent satellite and the collision probability for the tether itself. Because the methodology for handling the parent satellite has already been developed,[7] the focus of this work is on the collision probability of the tether itself.

Tracking of the tether introduces problems because of its very small diameter. Therefore, the tether is assumed to have the same state vector as the parent satellite. This assumption is valid because the position of the tether in space is determined by the position of the parent satellite and the configuration of the tether with respect to the parent satellite. As long as the tether's position is correct, the resulting collision probability will be correct. Because the tether is assumed to have a known orientation with respect to its parent satellite, the tether itself has the same error covariance matrix as the parent satellite.

The debris object and parent satellite are propagated to the point of closest approach. If proximity to the parent satellite is used as a criterion to determine if a probability calculation is warranted, then the threshold distance must account for the length of the tether. Because the relative velocity of orbital objects near closest approach is very large compared to the velocity change produced by the relative acceleration, the relative velocity can be considered constant during the encounter period.

The positional error of each object at closest approach is represented by a three-dimensional Gaussian probability density as shown in Fig. 1. The relative positional error of the objects can be obtained by simply adding the error covariance matrices. Because the objects pass each other at constant velocity, the three-dimensional probability density is reduced to a two-dimensional distribution. That is, the probability density as a function of position along the velocity direction can be integrated, yielding a two-dimensional Gaussian distribution in the encounter plane, which is normal to the relative velocity vector.

The collision probability is obtained by integrating the two-dimensional probability density over the appropriate collision cross section. The collision cross section depends on the tether configuration and size of the colliding space object.

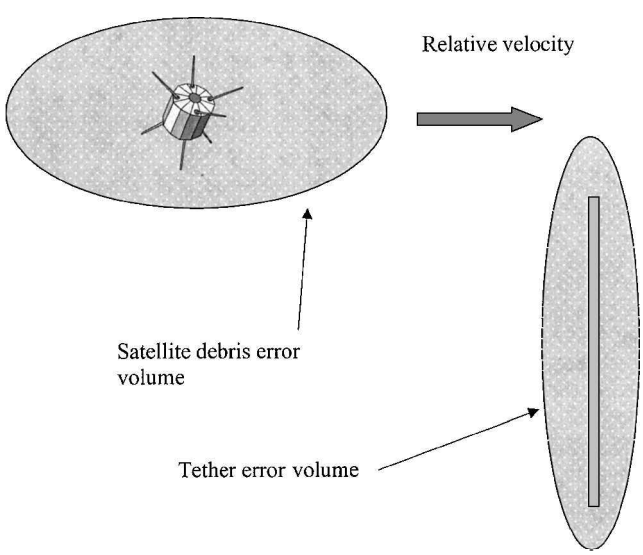

Fig. 1 Notional satellite debris and tether encounter geometry with three-sigma error volumes.

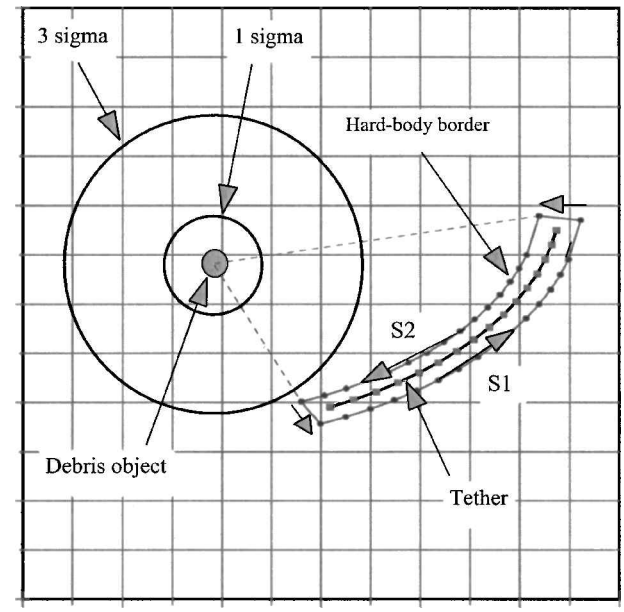

Fig. 2 Contour integration about tether hard body in symmetrized encounter plane.

It is assumed that the configuration of the tether is predetermined and specified as a series of points in the local frame of the parent satellite at the time of closest approach. These defining points are projected to the encounter plane. The combined tether/debris hard body is found by adding a border representing the size of the debris object and the tether radius. This is achieved by defining a new set of points lying on the perimeter of the combined hard-body area in the encounter frame.

All of the relative positional error can be attributed to the space object located at the origin of the encounter plane. The nominal relative displacement between the tether (parent satellite) and debris object in the encounter frame is added to each perimeter point so that the projected hard body is referenced to the origin of the probability density. If the actual relative separation distance between the tether and debris object lies within the projected hard body, a collision will occur. Therefore, the total probability is obtained by integrating the probability density within the surface bounded by the perimeter. The computation is simplified by performing a coordinate rotation and a scale change to make the probability density distribution symmetric. The coordinate rotation does not alter the shape of the surface, but changes its orientation and location. The subsequent scale change alters the hard-body shape. The scale change can be thought of as a change in integration variable. Because the integration limits are changed appropriately, the integration results are identical. The reason for changing the scale is to make the probability density symmetric. The symmetric form of the probability density enables integration over the radial parameter. This permits the two-dimensional integral over the hard-body area to be reduced to a one-dimensional path integral over the perimeter.

Figure 2 illustrates the contour integration about a tether hard body in the symmetrized encounter frame. The counterclockwise integration is indicated by the arrows along paths $S1$ and $S2$. The hard-body border was determined by the radius of the spherical space object shown at the origin. The radius of the colliding space object was increased for purposes of illustration. The probability density was made symmetric as indicated by the circular constant contour lines. This contour integration formulation simplifies the problem and enhances computation efficiency.

Analysis

The uncertainty in the relative position between the objects is defined by a three-dimensional Gaussian distribution given by

$$\rho(\boldsymbol{x}) = \left[1/(2\pi)^{\frac{3}{2}}\sigma_x\sigma_y\sigma_z\right]\exp\left[-\left(x^2/2\sigma_x^2\right) - \left(y^2/2\sigma_y^2\right) - \left(z^2/2\sigma_z^2\right)\right] \quad (1)$$

where σ_x, σ_y, and σ_z, are the standard deviations in positional error along each respective axis. When the distribution is transformed to the encounter frame and integrated along the relative velocity direction, which is taken to be along the Z axis, the three-dimensional Gaussian reduces to a two-dimensional Gaussian given by

$$h(\boldsymbol{x}) = \left[1/2^{\frac{3}{2}}\pi\sigma_x\sigma_y\sigma_z\sqrt{a}\right]\exp[-ex^2 - fy^2 - gxy] \quad (2)$$

The encounter coordinate frame in Eq. (2) is related to the frame defining the density in Eq. (1) by

$$\boldsymbol{x}_{\text{sigma}} = U\boldsymbol{x}_{\text{encounter}} \quad (3)$$

The parameters a, e, f, and g are defined in terms of the elements of U by

$$a = \frac{U_{13}^2}{2\sigma_x^2} + \frac{U_{23}^2}{2\sigma_y^2} + \frac{U_{33}^2}{2\sigma_z^2} \quad (4)$$

$$e = \frac{U_{11}^2}{2\sigma_x^2} + \frac{U_{21}^2}{2\sigma_y^2} + \frac{U_{31}^2}{2\sigma_z^2} - \frac{c^2}{4a} \quad (5)$$

$$f = \frac{U_{12}^2}{2\sigma_x^2} + \frac{U_{22}^2}{2\sigma_y^2} + \frac{U_{32}^2}{2\sigma_z^2} - \frac{d^2}{4a} \quad (6)$$

$$g = \frac{U_{11}U_{12}}{\sigma_x^2} + \frac{U_{21}U_{22}}{\sigma_y^2} + \frac{U_{31}U_{32}}{\sigma_z^2} - \frac{cd}{2a} \quad (7)$$

where

$$c = \frac{U_{11}U_{13}}{\sigma_x^2} + \frac{U_{21}U_{23}}{\sigma_y^2} + \frac{U_{31}U_{33}}{\sigma_z^2} \quad (8)$$

$$d = \frac{U_{12}U_{13}}{\sigma_x^2} + \frac{U_{22}U_{23}}{\sigma_y^2} + \frac{U_{32}U_{33}}{\sigma_z^2} \quad (9)$$

The collision probability density per unit area is given by $h(\boldsymbol{x})$ in Eq. (2). All of the uncertainty in relative position, which is represented by $h(\boldsymbol{x})$, can be assigned to the space object, which is located at the origin of the encounter frame.

The tether is represented by points lying on a curve that defines the tether's shape in the local frame of the parent satellite. The points are transformed to the encounter frame and projected to the encounter plane. These points have no positional uncertainty because all of the relative uncertainty has been attributed to the space object. A border is added to the points to account for the size of the space object and radius of the tether itself. The border is defined by a set of sequentially enumerated points $\boldsymbol{q}_i$ that traverse its perimeter in the counterclockwise direction as shown in Fig. 3. If the actual position of the space object lies within the region defined by $\boldsymbol{q}_i$, a collision will occur. Therefore, the collision probability is found by integrating the probability density over the hard-body area bounded by $\boldsymbol{q}_i$. A step function $u(\boldsymbol{x})$ can be used to define the region of integration, where $u(\boldsymbol{x}) = 1$ if $\boldsymbol{x}$ lies in the region bounded by $\boldsymbol{q}_i$ and $u(\boldsymbol{x}) = 0$ otherwise. The collision probability is obtained by integrating the product of $h(\boldsymbol{x})$ and $u(\boldsymbol{x})$, as given in Eq. (10),

$$P = \iint h(\boldsymbol{x})u(\boldsymbol{x})\,\mathrm{d}\boldsymbol{x} \quad (10)$$

The collision probability calculation can be greatly simplified by reducing the integration over the hard-body area to integration about a contour enclosing the area. This is achieved by performing a rotation followed by a scale change in the encounter plane so that the probability density can be made symmetric. Both the rotation and the scale change are changes in an integration variable that does not change the value of the integral.

A coordinate rotation is performed to eliminate the cross term in h to yield

$$h(\boldsymbol{x}) = \left[1/2^{\frac{3}{2}}\pi\sigma_x\sigma_y\sigma_z\sqrt{a}\right]\exp[-\alpha x^2 - \beta y^2] \quad (11)$$

where

$$\alpha = (e+f)/2 - \left[\sqrt{g^2 + (f-e)^2}\right]/2 \quad (12)$$

$$\beta = (e+f)/2 + \left[\sqrt{g^2 + (f-e)^2}\right]/2 \quad (13)$$

This rotation changes $\boldsymbol{q}_i$ to $\boldsymbol{q}_{ir}$ as given by

$$\boldsymbol{q}_{ir} = T\boldsymbol{q}_i \quad (14)$$

where T is given by

$$T = \begin{bmatrix} \cos(\phi) & \sin(\phi) \\ -\sin(\phi) & \cos(\phi) \end{bmatrix} \quad (15)$$

$$\cos(\phi) = \sqrt{\frac{1}{2}\left[1 - \frac{(f-e)}{\sqrt{g^2 + (f-e)^2}}\right]} \quad (16)$$

$$\sin(\phi) = \pm\sqrt{\frac{1}{2}\left[1 + \frac{(f-e)}{\sqrt{g^2 + (f-e)^2}}\right]} \quad (17)$$

The correct sign in Eq. (17) is determined by ensuring that the cross term in Eq. (11) is zero, that is,

$$2(f-e)\sin(\phi)\cos(\phi) + g[\cos(\phi)^2 - \sin(\phi)^2] = 0 \quad (18)$$

A scale change in the y axis is made to make $h(\boldsymbol{x})$ symmetric. This scale change is essentially a change in integration variable. The limits of integration are adjusted appropriately for the new integration variable:

$$y = \sqrt{(\alpha/\beta)}y' \quad (19)$$

$$h(\boldsymbol{x}) = \left(\sqrt{\alpha}/2^{\frac{3}{2}}\pi\sigma_x\sigma_y\sigma_z\sqrt{a\beta}\right)\exp[-\alpha x^2 - \alpha y'^2] \quad (20)$$

The y component of $\boldsymbol{q}_{ir}$, q_{ir} (2), is multiplied by a scale factor given by

$$q_{irs}(2) = \sqrt{(\beta/\alpha)}q_{ir}(2) \quad (21)$$

Using Eq. (20) in Eq. (10) and converting to polar coordinates, one finds

$$P = \frac{\sqrt{\alpha}}{2^{\frac{3}{2}}\pi\sigma_x\sigma_y\sigma_z\sqrt{a\beta}}\iint \exp(-\alpha r^2)r\,\mathrm{d}r\,\mathrm{d}\theta \quad (22)$$

The advantage of having a symmetric probability density function is now clear because the integration over r can be performed immediately, yielding

$$P = \frac{1}{2\pi}\left[\int_{s2}\exp(-\alpha r^2)\,\mathrm{d}\theta - \int_{s1}\exp(-\alpha r^2)\,\mathrm{d}\theta\right] \quad (23)$$

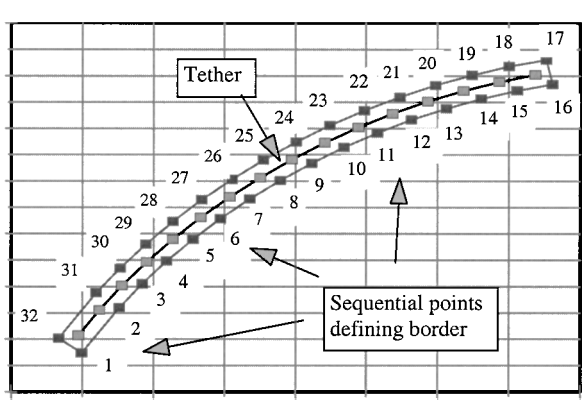

Fig. 3 Sequential points defining the integration region in the encounter plane.

where $s1$ and $s2$ are contours defining the hard-body area as shown in Fig. 2. For each value of θ, $s1$ and $s2$ define the contours that are farthest and closest to the origin, respectively. The usual integration technique involves solving for r for each value of θ along the contours $s1$ and $s2$ and determining the endpoints where $s1$ joins $s2$. These tedious computations can be avoided by noting that Eq. (23) is equivalent to the closed path integral defined by

$$P = \frac{-1}{2\pi} \oint \exp(-\alpha r^2)\, \mathrm{d}\theta \tag{24a}$$

(origin excluded from hard body)

$$P = 1 - \frac{1}{2\pi} \oint \exp(-\alpha r^2)\, \mathrm{d}\theta \tag{24b}$$

(origin included in hard body), where the minus sign is introduced to be consistent with integrating around the closed contour in the counterclockwise direction. If the origin, which is the nominal position of the space object, is contained in the hard body, the line integral includes an infinitesimal clockwise circle about the origin that contributes $a + 2\pi$ to the value of the integral. In this case, Eq. (24a) is replaced with Eq. (24b).

This simple contour integral involving only a scalar exponential in the integrand greatly increases computational efficiency. In addition, the ease of defining the closed contour enables the methodology to be applied to tethers of arbitrary shape and orientation.

Numerical Implementation

The evaluation of the path integral in Eq. (24) proceeds by considering two adjacent points, $\boldsymbol{x}_1$ and $\boldsymbol{x}_2$, that lie on the hard-body perimeter. The distance between $\boldsymbol{x}_1$ and $\boldsymbol{x}_2$ is divided into J subintervals defined by adjacent vectors, $\boldsymbol{X}'_n$ and $\boldsymbol{X}_n$, given by

$$\boldsymbol{X}'_n = [\boldsymbol{x}_2(n) + \boldsymbol{x}_1(J-n)]/J \tag{25}$$

$$\boldsymbol{X}_n = [\boldsymbol{x}_2(n-1) + \boldsymbol{x}_1(J-n+1)]/J \tag{26}$$

As n goes from 1 to J, the subinterval moves from $\boldsymbol{x}_1$ to $\boldsymbol{x}_2$. The angle between the two vectors $\mathrm{d}\theta_n$ is found by noting its relationship to the cross product between the two vectors:

$$\boldsymbol{X}_n \times \boldsymbol{X}'_n = |\boldsymbol{X}_n||\boldsymbol{X}'_n| \sin(\mathrm{d}\theta_n) \tag{27}$$

After rearranging Eq. (27), one finds

$$\mathrm{d}\theta_n = \sin^{-1}\left(\frac{\boldsymbol{X}_n \times \boldsymbol{X}'_n}{|\boldsymbol{X}_n||\boldsymbol{X}'_n|}\right) \tag{28}$$

The integrand is the average of its endpoint values:

$$I_n = \left\{\exp\left[-\alpha(\boldsymbol{X}_n)^2\right] + \exp\left[-\alpha(\boldsymbol{X}'_n)^2\right]\right\}/2 \tag{29}$$

The integral is evaluated by summing the product of I_n and $\mathrm{d}\theta_n$ for each subinterval between points $\boldsymbol{x}_1$ and $\boldsymbol{x}_2$:

$$P_i = \sum_{n=1}^{J} I_n\, \mathrm{d}\theta_n \tag{30}$$

where the index i indicates the particular pair of points $\boldsymbol{x}_1$ and $\boldsymbol{x}_2$. The same procedure is performed for each of the N pairs of sequential points as the hard-body perimeter is traversed in the counterclockwise direction as illustrated in Fig. 3. The contributions are summed to obtain the total collision probability between the tether and space object:

$$P = \frac{-1}{2\pi} \sum_{i=1}^{N} P_i \tag{31a}$$

(origin excluded from hard body)

$$P = 1 - \frac{1}{2\pi} \sum_{i=1}^{N} P_i \tag{31b}$$

(origin included in hard body).

Note that more sophisticated numerical integration schemes could be applied if needed.

Numerical Results

The computation technique for a space tether was implemented on a computer and test cases were run. Table 1 contains state vectors and error covariance matrices of two space objects. The closest approach distance between the objects is 75.38 km. A 20-km tether was extended from object number one located at the origin in Fig. 4. Four different configurations of the tether were examined, as illustrated in Fig. 4. The curved tether configurations are 20 km in length and shaped as circular arcs each having radius of curvature of 20 km. By the use of the state vectors and error covariance matrices in Table 1, the collision probability between an object of given radius and each tether configuration was computed. The state vector and error covariance matrix of each tether was assumed identical to the parent satellite. A border was place about each tether, based on the object radius, as illustrated in Fig. 3. The collision probability results for object radii ranging from 0.5 to 5.0 m are presented in Fig. 5. Tether collision probabilities were several hundred times larger than those for a sphere having a radius of 6 m, as shown in Fig. 5.

A set of 22 state vectors and associated covariance matrices were used to calculate the collision probability between a space object having a 1-m radius and a 20-km tether. The tether was extended above the parent object as in case 2 of Fig. 4. Table 2 presents the collision probability results and a comparison to a sphere having a radius of 6 m. Each trajectory pair has a different miss range as shown in Table 2. The fractional increase the tether's collision probability over that of the sphere is also presented in Table 2. Figure 6 illustrates the tether's increased collision probability over that of the sphere in graphical form.

The collision probability for each of the 22 state vectors and error covariance matrices were calculated all four tether configuration shown in Fig. 4. The results are presented in Table 3, where the probability averages for all four configurations are included. Figure 7 illustrates the effect of tether configuration on the collision

Table 1 State vector and error covariance matrices used to compute collision probabilities in Fig. 5

Vehicle/covariance number	X	Y	Z
		Position	
Vehicle 1	−913.562131	6,630.404542	−2,929.713881
Vehicle 2	−855.377006	6,620.480899	−2,976.591167
		Velocity	
Vehicle 1	−1.367889	2.724617	6.707462
Vehicle 2	−10.459621	0.794638	−4.168832
		Covariance	
Covariance 1	448.818323	−727.075958	−1,660.710398
Covariance 1	−727.075958	1,742.760413	3,265.600052
Covariance 1	1,660.710398	3,265.600052	8,308.421264
Covariance 2	16,209.600283	−1,397.837101	4,314.897605
Covariance 2	−1,397.837101	1,965.958018	3,060.570365
Covariance 2	4,314.897605	3,060.570365	11,462.028460

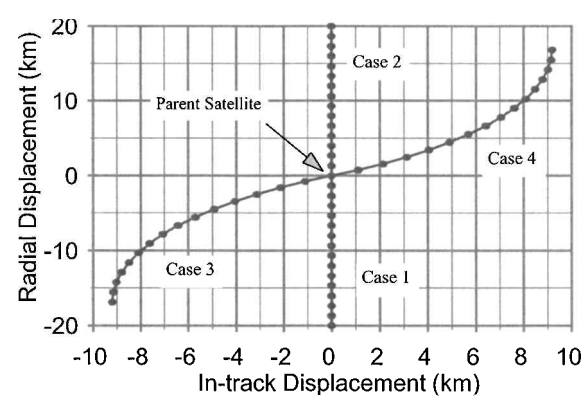

Fig. 4 Four tether configurations with respect to the parent satellite.

Table 2 Collision probability comparison for various trajectory cases involving a 1-m radius sphere vs a 6-m radius sphere and a 1-m-radius sphere vs a 20-km tether

Trajectory case number	Miss range, km	Sphere, 6 m	Tether, 20 km	Fractional increase
1	75.38	4.34e−9	1.20e−6	276.8
2	59.82	6.76e−9	1.40e−6	206.5
3	67.43	4.48e−9	1.01e−6	224.6
4	46.03	2.95e−9	3.29e−7	111.3
5	86.65	3.85e−9	1.13e−6	294.3
6	78.48	6.21e−9	1.81e−6	291.5
7	23.68	5.44e−9	1.49e−6	273.3
8	48.93	3.83e−9	1.08e−6	282.7
9	123.61	3.58e−9	8.08e−7	226.1
10	80.14	7.29e−9	1.65e−6	225.8
11	45.26	6.87e−9	1.69e−6	245.7
12	66.09	2.12e−9	4.43e−7	208.8
13	78.31	3.16e−9	5.98e−7	189.2
14	29.49	5.86e−9	1.85e−6	315.3
15	59.92	3.74e−9	1.05e−6	282.1
16	42.66	7.68e−9	1.87e−6	243.8
17	140.07	3.10e−9	7.17e−7	231.0
18	45.21	4.00e−9	1.15e−6	286.2
19	85.42	3.71e−9	7.69e−7	207.2
20	33.99	3.12e−9	9.93e−7	302.0
21	17.70	4.28e−9	1.19e−6	278.5
22	3.91	7.23e−9	1.61e−6	223.3

Table 3 Collision probabilities for various trajectory cases and tether configurations

Case	Miss range, km	Tether 1	Tether 2	Tether 3	Tether 4	Average
1	75.38	8.84e−7	1.20e−6	9.63e−7	1.18e−6	1.06e−6
2	59.82	1.69e−6	1.40e−6	1.72e−6	1.53e−6	1.58e−6
3	67.43	1.14e−6	1.01e−6	1.14e−6	1.07e−6	1.09e−6
4	46.03	3.15e−7	3.29e−7	2.32e−7	2.44e−7	2.80e−7
5	86.65	7.60e−7	1.13e−6	8.20e−7	1.07e−6	9.47e−7
6	78.48	1.13e−6	1.81e−6	1.19e−7	1.81e−6	1.48e−6
7	23.68	1.15e−6	1.49e−6	1.19e−7	1.47e−6	1.32e−6
8	48.93	7.54e−7	1.08e−6	8.35e−7	1.09e−6	9.39e−7
9	123.61	8.64e−7	8.08e−7	9.34e−7	8.36e−7	8.61e−7
10	80.14	1.67e−6	1.65e−6	1.76e−6	1.65e−6	1.68e−6
11	45.26	1.31e−6	1.69e−6	1.48e−6	1.76e−6	1.56e−6
12	66.09	6.28e−7	4.43e−7	6.29e−7	4.63e−7	5.41e−7
13	78.31	9.59e−7	5.98e−7	9.63e−7	6.46e−7	7.91e−7
14	29.49	9.96e−7	1.85e−6	1.11e−6	1.78e−6	1.43e−6
15	59.92	7.39e−7	1.05e−6	8.20e−7	1.05e−6	9.16e−7
16	42.66	1.65e−6	1.87e−6	1.72e−6	1.95e−6	1.80e−6
17	140.07	7.48e−7	7.17e−7	8.10e−7	7.29e−7	7.51e−7
18	45.21	8.04e−7	1.15e−6	8.60e−7	1.15e−6	9.90e−7
19	85.42	9.97e−7	7.69e−7	9.98e−7	8.50e−7	9.03e−7
20	33.99	6.05e−7	9.93e−7	6.60e−7	9.30e−7	7.85e−7
21	17.70	8.77e−7	1.19e−6	9.44e−7	1.20e−6	1.05e−6
22	3.91	1.53e−6	1.61e−6	1.34e−6	1.39e−6	1.47e−6

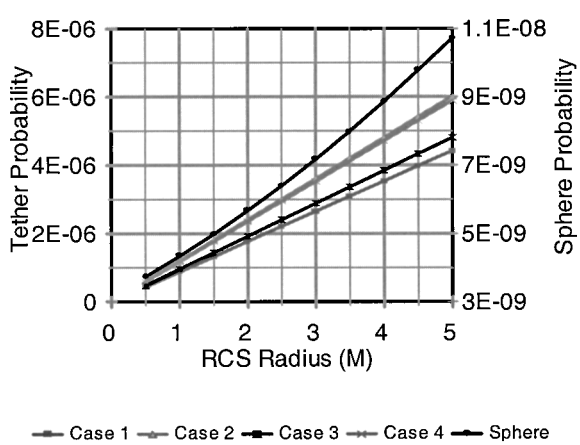

Fig. 5 Collision probability between tethers defined in Fig. 4 and a variable size object.

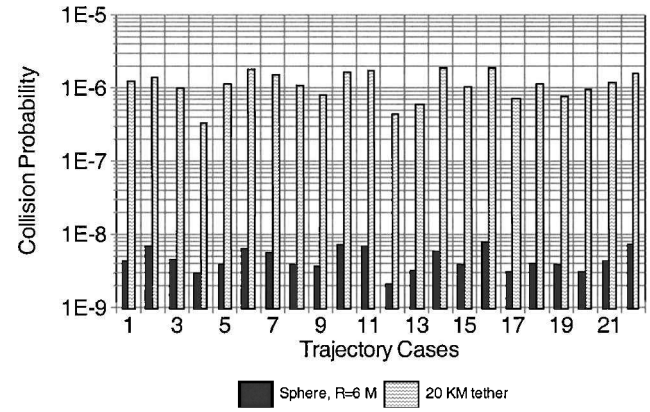

Fig. 6 Tether's increased collision probability over that of a 6-m-radius sphere from data in Table 2.

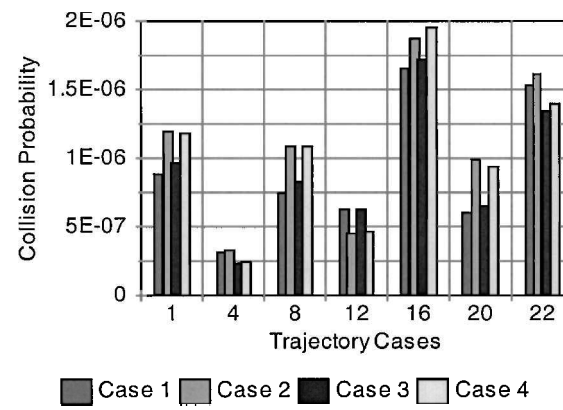

Fig. 7 Effect of tether configuration on collision probability from data in Table 3.

probability. The probabilities differ by much less than an order of magnitude. These results suggest that large uncertainty in tether configuration due to the complex dynamics will not significantly degrade the accuracy of collision probability prediction.

The numerical results indicate that the collision probability associated with a space tether is several hundred times larger than that of a space object 6 m in radius. This result is consistent with a recent statistical study of tether collision probability.[12] The statistical study also found that collision probability associated with tethers is large.

Conclusions

A general method for calculating collision probability between a space tether and a space object was developed. The tether hard body was modeled as a long serpentine shape with a negligible diameter. The space object was assumed to be spherical in shape. The collision probability depends on the associated state vectors and error covariance matrices, as well as the size of the space object and deployment configuration of the tether. The probability calculation was reduced to evaluating a one-dimensional contour integral about the perimeter of the tether hard-body area. The methodology is applicable to tethers of arbitrary configuration and is amenable to computer implementation. Numerical test results indicate that tethers several kilometers in length have collision probabilities much greater than those of typical satellites.

References

[1]Reynolds, R., Eichler, P., and Johnson, N., "An Overview of Revised NASA Safety 1740.14," *Proceedings of the Second European Conference on Space Debris*, ESA, Noordwijk, The Netherlands, 1997, pp. 721–726.

[2]Chobotov, V. A., and Mains, D. L., "Tether Satellite System Collision Study," *Space Debris*, Vol. 1, No. 2, 1999, pp. 99–112.

[3]Chan, K., "Collision Probability Analysis for Earth Orbiting Satellites," *Advances in the Astronautical Sciences*, Vol. 96, 1997, pp. 1033–1048.

[4]Berend, N., "Estimation of the Probability of Collision Between Two Catalogued Orbiting Objects," *Advances in Space Research*, Vol. 23, No.1, 1999, pp. 243–247.

[5]LeClair, R. A., "Probability of Collision in the Geostationary Orbit," *Proceedings of the 2000 Space Control Conference*, Lincoln Lab., Massachusetts Inst. of Technology, Lexington, MA, 2000, p. 85.

[6]Alfriend, K. T., Akella, M. R., Lee, D., Frisbee, J., and Foster, J. L., "Probability of Collision Error Analysis," *Space Debris*, Vol. 1, No. 1, 1999, pp. 21–35.

[7]Patera, R. P., "General Method for Calculating Satellite Collision Probability," *Journal of Guidance, Control, and Dynamics*, Vol. 24, No. 4, 2001, pp. 716–722.

[8]Misra, A. K., and Modi, V. J., "A Survey on the Dynamics and Control of Tethered Satellite Systems," *Advances in the Astronautical Sciences*, Vol. 62, 1987, pp. 667–719.

[9]Beletsky, V. V., and Levin, E. M., "Dynamics of Space Tether Systems," *Advances in the Astronautical Sciences*, Vol. 83, 1993, pp. 61–114.

[10]Keshmiri, M., Misra, A. K., and Modi, V. J., "General Formulation for *N*-Body Tethered Satellite System Dynamics," *Journal of Guidance, Control, and Dynamics*, Vol. 19, No. 1, 1996, pp. 75–83.

[11]Kalantzis, S., Modi, V. J., Pradhan, S., and Misra, A. K., "Order-*N* Formulation and Dynamics of Multibody Tethered Systems," *Journal of Guidance, Control, and Dynamics*, Vol. 21, No. 2, 1998, pp. 277–285.

[12]Cooke, W. J., Spencer, D. B., Anderson, B. J., and Suggs, R. M., "Tether Survivability and Collision Avoidance: Is LEO the Right Place for Tethered Systems?," STAIF-2001, Space Technology and Applications International Forum, Feb. 2001.